Colloids and Surfaces B: Biointerfaces 145 (2016) 291–300

Contents lists available at ScienceDirect

Colloids and Surfaces B: Biointerfaces

journal homepage: www.elsevier.com/locate/colsurfb

Surface modification with zwitterionic cysteine betaine for nanoshell-assisted near-infrared plasmonic hyperthermia

Chun-Jen Huang[a,b,*], Sz-Hau Chu[a], Chien-Hung Li[c], T. Randall Lee[c]

[a] Department of Biomedical Sciences and Engineering, National Central University, Jhong-Li, Taoyuan 320, Taiwan
[b] Department of Chemical and Materials Engineering, National Central University, Jhong-Li, Taoyuan 320, Taiwan
[c] Department of Chemistry and the Texas Center for Superconductivity, University of Houston, Houston, TX 77204-5003, United States

ARTICLE INFO

Article history:
Received 5 February 2016
Received in revised form 17 April 2016
Accepted 4 May 2016
Available online 4 May 2016

Keywords:
Zwitterionic materials
Antifouling coating
Nanomaterials
Hyperthermia
Bioinspired materials
Cancer therapy

ABSTRACT

Nanoparticles decorated with biocompatible coatings have received considerable attention in recent years for their potential biomedical applications. However, the desirable properties of nanoparticles for in vivo uses, such as colloidal stability, biodistribution, and pharmacokinetics, require further research. In this work, we report a bio-derived zwitterionic surface ligand, cysteine betaine (Cys-b) for the modification of hollow gold-silver nanoshells, giving rise to hyperthermia applications. Cys-b coatings on planar substrates and nanoshells were compared to conventional (11-mercaptoundecyl)tri(ethylene glycol) (OEG-thiol) to investigate their effects on the fouling resistance, colloidal stability, environmental tolerance, and photothermal properties. The results found that Cys-b and OEG-thiol coatings exhibited comparable antifouling properties against bacteria of gram-negative *Pseudomonas aeruginosa* (*P. aeruginosa*) and gram-positive *Staphylococcus epidermidis* (*S. epidermidis*), NIH-3T3 fibroblasts, and bovine serum albumin. However, when the modified nanoshells were suspended at a temperature of 50 °C in aqueous 3 M NaCl solutions, shifts in the extinction maximum of the OEG-capped nanoshells with time were observed, while the corresponding spectra of nanoshells capped with Cys-b generally remained unchanged. In addition, when the nanoshells were continuously exposed to NIR irradiation, the temperature of the solution containing nanoshells capped with Cys-b increased to a plateau of 54 °C, while that of the OEG-capped nanoshells gradually decreased after reaching a peak temperature. Accordingly, the Cys-b nanoshells were conjugated with anti-HER2 antibodies for targeted delivery to HER2-positive MDA-MB-453 breast cancer cells for hyperthermia treatment. The results showed the selective delivery and effective photothermal cell ablation with the antibody-conjugated Cys-b nanoshells. Therefore, this work demonstrated the promise of bio-derived zwitterionic Cys-b as a stable and biocompatible surface coating for materials in nanomedicine.

1. Introduction

Hyperthermia, which involves the introduction of moderate heat to a specific target, has become an important method for tumor therapy because of the limited tolerance of tumor cells to a temperature range of 41–47 °C [1,2]. These elevated temperatures cause irreversible cell damage by loosening cell membranes and denaturing proteins. The heating sources applied include radio frequency, microwaves, and ultrasound waves. However, these sources suffer from drawbacks because of their associated damage to the surrounding healthy tissues. An alternative strategy is photothermal therapy (PTT) in which photothermal agents are employed for heat generation in a local environment [3–6]. The agents can be dye molecules such as naphthalocyanines, indocyanine, and porphyrins coordinated to transition metals. However, these chromophores suffer from low absorption coefficients and poor photostability [7,8]. In recent years, tremendous advances have been witnessed in the development of nanomaterials with unique optical properties [9–11]. More specifically, novel metal nanoparticles have been employed as powerful agents for PTT because of their robust photostability and strong optical response via the surface plasmon resonance (SPR). A variety of plasmonic nanostructures including nanospheres [12,13], nanoshells [14,15], nanorods [16,17], and nanocages [18], have been developed that respond to wavelengths in the visible and near infrared (NIR) regions. In PTT applications, in addition to a strong extinction, the nanoparticle agents should possess additional properties, such as nontoxicity, long-term colloidal

* Corresponding author at: Department of Biomedical Sciences and Engineering, National Central University, Jhong-Li, Taoyuan 320, Taiwan.
E-mail address: cjhuang@ncu.edu.tw (C.-J. Huang).

http://dx.doi.org/10.1016/j.colsurfb.2016.05.004
0927-7765/

stability, high biocompatibility, and facile functionalization [19]. These requirements shed light on the critical role of surface chemistry for decorating plasmonic nanomaterials for their effective and safe implementations.

Commonly, thiolated oligo(ethylene glycol) (OEG) adsorbates are employed as capping ligands, in which thiol groups are adsorbed onto the surface of gold nanostructures via thiol-gold bonds [20]. OEG-modified nanoparticles can significantly enhance colloidal stability, biocompatibility, and biodistribution [21]. Because of its steric repulsion with an elastic and osmotic component [22–24], OEG coatings serve as antifouling materials to repel nonspecific adsorptions. Nevertheless, several factors must be considered when using OEG coatings under complex conditions [24]. For example, OEG adsorbates form hydrogen bonds with water molecules, and thus the conformational change and packing density of the oligomeric ethylene glycol can significantly affect the interfacial water layers [25]. In addition, enhanced temperature and ionic strength in the environment induce changes in the OEG conformation from a helical to an all-trans form, which leads to weakening of the bonding to interfacial water molecules [26]. Furthermore, the poor hydration of OEG eventually gives rise to energetically favorable nonspecific adsorptions [27]. Additionally, OEG can undergo degradation under the stresses of heat and light irradiation, and the possible formation of hydroperoxides [21,28,29]. Taken together, an alternative coating material to OEG for use in particular cases, such as plasmonic nanoparticles for the photothermal therapy, remains highly desirable.

In recent years, attention has been paid to zwitterionic materials, which contain both positively and negatively charged groups. These materials interact strongly with water molecules through ionic solvation, leading to stable configurations at high temperature and ionic strength [27,30–33]. Analogously, in nature, cell membranes are comprised largely of amphiphilic lipids containing polar zwitterionic groups that resist nonspecific adsorptions and allow highly selective biorecognition at interfaces. Therefore, an increasing number of applications utilizing zwitterionic materials as biocompatible and antifouling coatings for complex environments have been explored [30,31,34–36]. Our group recently reported the study and development of a novel zwitterionic surface ligand, cysteine betaine (Cys-b), which is derived from the natural organosulfur compound, cysteine, by converting its primary amine to a quaternary ammonium [37]. We showed that this branched zwitterionic group has a high tolerance to pH changes and resistance to photooxidation in the presence of oxygen and light irradiation [37]. Moreover, self-assembled monolayers (SAMs) of Cys-b on gold exhibit better repellence than cysteine against proteins, bacteria, and mammalian cells. Therefore, the unique features of Cys-b make it promising as a new nanoscale coating material for potential implementation in the modification of plasmonic nanomaterials for PTT.

In the research reported here, we conducted a comparative study between Cys-b and thiolated OEG coatings on both planar "flat" gold surfaces and on plasmonic gold-based nanoparticles. The formation of SAMs on the flat gold surfaces was examined by contact angle measurements and X-ray photoelectron spectroscopy (XPS). Fouling tests on modified substrates were carried out with protein, bacteria, and NIH 3T3 cells. Importantly, the colloidal stability of plasmonic hollow gold-silver nanoshells coated with Cys-b and OEG-thiol was investigated by UV–vis spectroscopy and dynamic light scattering (DLS) to follow the changes in light absorbance/scattering and hydrodynamic sizes, respectively. The photothermal properties of modified nanoparticles as PTT agents were confirmed by NIR irradiation and the measurement of temperature changes in solutions. Finally, we demonstrated the effectiveness of Cys-b modified hollow gold-silver nanoshells conjugated with anti-HER2 antibodies against MDA-MB-453 breast cancer cells in hyperthermia treatments. These studies provided not only insight into the potential benefits of Cys-b as a zwitterionic surface ligands for plasmonic nanoparticles, but also evidence of a robust surface strategy for maintaining bioinertness in complex environments.

2. Experimental section

2.1. Materials

L-Cysteine, potassium hydroxide (KOH), dimethyl sulfate, trifluoroacetic acid (TFA), glacial acetic acid, acetone, silver nitrate, potassium carbonate, N-hydroxysuccinimide (NHS), and (1-ethyl-3-(3-dimethylaminopropyl)carbodiimide) (EDC) were purchased from Sigma-Aldrich. (11-Mercaptoundecyl)tri(ethylene glycol) (OEG-thiol) and thiol-PEG6-acid (COOH-thiol) were purchased from Broadpharm. Anti-HER2 mouse antibodies and anti-mouse IgG (H + L) conjugated with Alexa Fluor 488 were obtained from Cell Signaling Technology. Trisodium citrate dihydrate and nitric acid were obtained from EM Science. Hydrogen tetrachloroaurate(III) hydrate ($HAuCl_4 \cdot H_2O$) was purchased from Strem. Bovine serum albumin (BSA) was obtained from MDBio Inc. Dulbecco's Modified Eagle's Medium (DMEM) and fetal bovine serum (FBS) were obtained from Gibco. LIVE/DEAD Viability/Cytotoxicity Kit containging calcein AM and EthD-1 was purchased from Thermo Fisher Scientific. Luria-Bertani broth (LB broth) was obtained from BD. Water was purified to a resistivity of 18 MΩ·cm using the Academic Milli-Q Water System (Millipore Corporation) and filtered using a 0.22 μm filter.

2.2. Cys-b synthesis

The detailed experimental procedure for Cys-b synthesis has been described [37]. Briefly, a flask containing 1 g of cysteine in 3 mL of deionized water was immersed in an ice bath and stirred under nitrogen. An 8.5 mL aliquot of 6.5 M KOH was introduced dropwise until the cysteine dissolved. The residual KOH and 5.2 mL of dimethyl sulfate were dropped in simultaneously over 1 h with stirring. Afterward, the flask was kept for another 20 min at rt, and then 1.2 mL of glacial acetic acid was added. The solution was evaporated *in vacuo* to a volume of around 2 mL. The byproduct potassium methyl sulfate was precipitated by adding 40 mL of ethanol and then filtered. The filtrate was concentrated using a rotovap to a volume of around 2 mL, and then precipitated by adding 50 mL of acetone. The white product was washed with acetone 5 times to afford pure cysteine betaine, which was reduced in 0.1 M dithiothreitol (DTT) in deionized water and stirred at 65 °C for 2 h. After cooling, 50 mL of acetone was added to precipitate the white product of pure Cys-b (70% yield).

2.3. Formation of SAMs on planar substrates

Au thin films with a thickness of 50 nm on glass slides were prepared by thermal evaporation (I Shien SPS-302). The substrates were cleaned in a sonication bath of 0.1% SDS, acetone, and ethanol for 10 min of each, followed by drying under a stream of nitrogen. The substrates were transferred to a plasma cleaner (PDC-001, Harrick Plasma, NY) to expose O_2 plasma twice with a power of 10.5 W for 10 min. The clean substrates were immediately immersed into a 1 mM Cys-b solution in DI water containing 2% TFA or 1 mM OEG-thiol solution in ethanol, and shaken at 50 rpm at room temperature for 12 h. The modified substrates were removed and cleaned with deionized water, ethanol, and water, followed by drying under a stream of nitrogen [38].

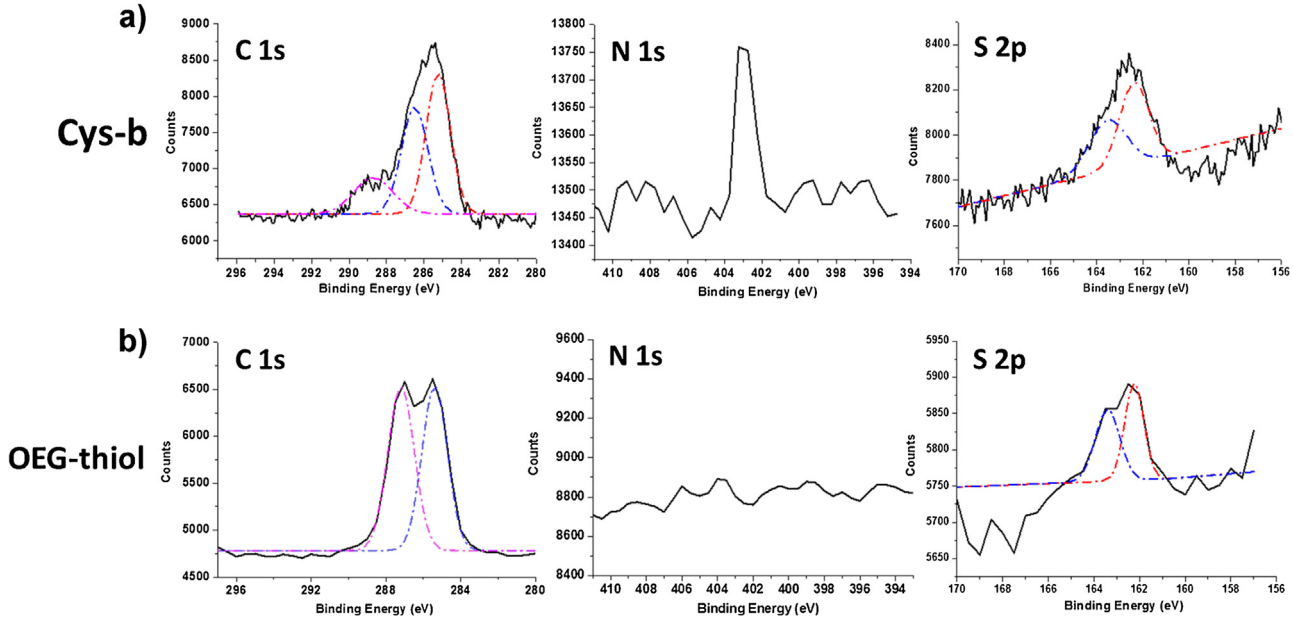

Fig. 1. XPS spectra of C 1s, N 1s, and S 2p regions for SAMs derived from (a) Cys-b and (b) OEG-thiol. The SAMs were prepared on planar evaporated Au substrates.

2.4. Contact angle measurements

Static water contact angles were accessed by using an optical contact angle goniometer (Phoenix mini, Surface Electro Optics, Seoul). The 5 μL water droplets from a microsyringe were placed on the flat gold substrates, and the contact angles were measured at least three times at random positions.

2.5. XPS measurements

The elemental spectra were detected by XPS with a microfocused and monochromatic Al Kα X-ray source (1486.6 eV, 400 μm; Sigma Probe, Thermo Scientific). The takeoff angle (with respect to the surface) of the photoelectron was set at 45°. The pressure of the system was below 10^{-10} Pa using an oil-less ultrahigh vacuum pumping system. A dual beam charge neutralizer (7 V Ar^+ and flooding 3 kV, 1 μA electron beam) was employed to compensate for charging effects. Spectra were collected with a pass energy set to 58.7 eV, while the binding energy measured was calibrated against the Au 4f peaks at 84 and 88 eV. The typical data acquisition time was around 30 min.

2.6. Bacterial fouling tests

After inoculation for 16 h in LB in a conical flask at 37 °C shaking at 200 rpm, the bacteria of *S. epidermidis* or *P. aeruginosa* were then washed with sterile PBS for three times through centrifugation at 4000 rpm for 5 min and re-suspension in PBS. After the final wash, the bacterial samples in PBS were diluted to an optical density reading at 670 nm (OD670) of 0.1, corresponding to ~8×10^7 cells/mL, for testing the antifouling properties of substrates modified with OEG-thiol and Cys-b. The substrates were dipped into the bacterial solution at 37 °C for 3 h, followed by washing with PBS and shaking at 100 rpm for 5 min for three times. The adsorbed bacteria were stained with 50 μL of LIVE/DEAD BacLight for 15 min. Afterward, the substrates were observed using fluorescence microscopy (ZEISS Microscope Axio Obserber A1, Germany) with a magnification of 400 × and an excitation wavelength of 488 nm. The measurements were performed at five random locations on each sample, and the bacteria numbers were analyzed using an ImageJ software package (developed at National Institutes of Health, MA).

2.7. Cell adhesion tests

3T3 fibroblasts were maintained in DMEM with 10% FBS at 37 °C in an incubator with 95% relative humidity and 5% CO_2. The bare Au substrates and Au substrates modified with Cys-b and OEG-thiol were sterilized in 75% ethanol for 30 s and then washed with PBS for 3 min before cell seeding. The substrates were placed in a 24-well plate, and 3T3 fibroblasts in DMEM with 1% FBS were introduced with a total cell number of 2×10^5 per well. After culture for 72 h, the substrates were washed with PBS, followed by imaging using an optical microscopy. The cell number and cell coverage area were estimated using ImageJ software.

2.8. Preparation of gold-silver nanoshells

Silver nanoparticles were prepared using the method of Lee and Meisel [39]. Briefly, an aliquot of $AgNO_3$ (0.0340 g, 0.200 mmol) was dissolved in 200 mL of H_2O. The solution was brought to reflux, and then 4 mL of 1% trisodium citrate solution was added under vigorous stirring. The solution continued to reflux for 25 min. The contents turned a yellow green color, indicating the presence of silver nanoparticles. The solution was allowed to cool to rt and then centrifuged at 6000 rpm for 15 min. The nanoparticles were then re-dispersed in 25 mL of water. This procedure generated monodispersed silver nanoparticles, where the size could be adjusted from 40 nm to 100 nm, depending on the concentration of the reactants. For the synthesis of hollow gold-silver nanoshells as described in previous studies [15,40,41], 0.050 g of K_2CO_3 was added to 200 mL of purified water, which was then injected into 4 mL of 1% $HAuCl_4 \cdot H_2O$ solution. The mixture, initially yellow in color, became colorless 30 min after the reaction was initiated. The flask was then covered with aluminum foil to shield it from light, and the solution was stored in a refrigerator overnight. To obtain surface plasmon resonance (SPR) maxima centered at ~800 nm using the gold-silver nanoshell solutions, 20 mL of silver nanoparticles solution were mixed with 200 mL K-gold solution and stirred for 4 h. The SPR band of the solution was tracked using UV–vis

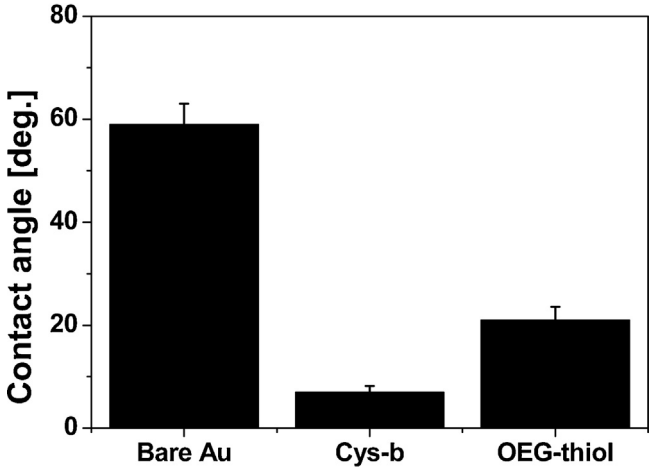

Fig. 2. The static contact angles on bare Au and Au modified with Cys-b and OEG-thiol. The measurements were performed at least three times for each sample.

measurements. The nanoshells were isolated by centrifugation at 6000 rpm for 15 min, and the supernatant was then decanted. The particles were re-dispersed in 22.5 mL water. The size and morphology of the nanoparticles were evaluated using a LEO-1525 scanning electron microscope (SEM, Carl Zeiss, Germany, Fig. S1 in Supplementary data) operating at an accelerating voltage of 15 kV and dynamic light scattering (DLS, Nano-S, Malvern, UK). The mean diameter of the nanoshells was 102 ± 21 nm. The concentration of nanoshells obtained from nanoparticle tracking analysis technology (NanoSight NS300, Malvern, UK) and the measured nanoshells concentration was $\sim 10^{11}$ nanoparticles/mL. Extinction spectra were collected over the wavelength range of 200–1000 nm with all nanoshell samples suspended in PBS for the measurements.

2.9. Colloidal stability tests

For the nanoshell modification, the total amount of the ligands, Cys-b and OEG-thiol, was 10^7 equivalent to nanoshells in deionized water by ligand exchange. The modification process was conducted for 12 h at rt, followed by collecting and washing with PBS via centrifugation at 9000 rpm for 10 min. The particles were re-suspended in PBS. The changes in maximum extinction peak and particle sizes were monitored using UV–vis spectroscopy and DLS. With regard to the effects of protein fouling, the nanoshell solutions were diluted 5 times at a concentration of $\sim 2 \times 10^{10}$ nanoshells/mL were prepared. BSA protein was added to the nanoshell solutions to a concentration of 4.9 mg/mL and the changes in the hydrodynamic size of nanoshells as a function of time were followed by dynamic light scattering (DLS, SZ-100, Horiba) measurements. To verify the colloidal stability of modified nanoshells in the presence of high ionic strength and heat, the nanoshells modified with Cys-b and OEG-thiol were dissolved in 3 M NaCl solution, and the temperature was maintained at 50 °C. The extinction spectra were recorded for 24 h using the UV–vis spectroscopy.

2.10. Antibody conjugation

For targeted hyperthermia applications with the nanoshells, anti-HER2 mouse monoclonal antibody was used to conjugate onto the nanoshells for delivery to HER2-positive MDA-MB-453 cell line. MDA-MB-453 cells were maintained in DMEM supplemented with 10% FBS at 37 °C in a humidified CO_2 incubator. In the beginning, the nanoshells were modified with carboxyl group termination by mixing COOH-thiol with Cys-b or OEG-thiol at a mole ratio of 1:4, respectively. The as-prepared nanoshells in DI H_2O at a concentration of $\sim 2 \times 10^{10}$ nanoshells/mL were treated with the mixed thiol solutions at a total concentration of 5 μM at rt for 48 h. After ligand exchange, the COOH-functionalized nanoshells were collected by centrifugation at 20,000 rpm for 10 min and redispersed in PBS. The carboxyl groups were activated by EDC/NHS amine coupling chemistry. The activation solution was prepared from dissolving 18 mg of EDC and 1.2 mg of NHS in 1 mL of PBS. A 1 mL aliquot of the activation solution was transferred to the modified-nanoshells solution at a concentration of $\sim 2 \times 10^{10}$ nanoshells/mL in PBS at 4 °C for 2 h. Afterward, the activated nanoshells were collected by centrifugation at 20,000 rpm for 10 min and washing three times with fresh PBS to remove unreacted chemicals. The activated nanoshells at a concentration of $\sim 2 \times 10^{10}$ nanoshells/mL were incubated with anti-HER2 Ab at a concentration of 1 μg/mL in PBS at rt for 3 h for protein conjugation. The anti-HER2 Ab-conjugated nanoshells were collected by centrifugation at 20,000 rpm for 10 min and washing three times with fresh PBS to remove free antibodies. The conjugated nanoshells were stored in a refrigerator at 4 °C and used for cell studies within one week. The presence of the anti-HER2 Ab on nanoshells was confirmed by adding anti-mouse IgG (H + L) conjugated with Alexa Fluor 488 and probing the fluorescence signal with a multi-detection microplate reader (Synergy HT, Biotek, VT). In addition, Fourier transform infrared spectroscopy (FTIR) was applied to identify the presence of proteins after conjugation (Fig. S2 in Supplementary data). It was estimated by the previous reports that the binding capacities of proteins on nanoparticles are in a range of 44–90 μg per mg NPs [42–44].

2.11. Hyperthermia tests

HER2-positive MDA-MB-453 breast tumor cells and HER2-negative NIH 3T3 fibroblasts were seeded onto a 96-well plate at a density of 10,000 cells per well for 2 days before the tests. The cells were washed three times with PBS, followed by incubation with nanoshells both with and without anti-HER2 Ab at 37 °C for 2 h. After incubation, the cells were irradiated with a NIR laser having a wavelength centered at 808 nm at an output power of 2.3 W/cm^2 for 10 min. The cells were then washed with PBS and stained with calcein AM for visualization of live cells and with EthD-1 for visualization of dead cells. Software ImageJ was applied to quantify the cell death percentage after exposure to NIR irradiation.

3. Results and discussion

3.1. SAM formation on planar substrates

To compare the interfacial properties of Cys-b and OEG-thiol SAMs, the adsorbates were dissolved in solvents and allowed to form SAMs on flat Au substrates. Because of the interplane electrostatic forces, the oppositely charged ions between amphoteric amino acids can interact to form a multilayer structure, leading to an unbalanced interfacial charge and incomplete formation of monolayers [45]. Therefore, we prepared Cys-b SAMs using treatments of TFA to disrupt the interplane electrostatic forces between free and bound molecules on the surface [37,46]. Elemental compositions and interfacial wettability of the SAMs were determined by XPS analysis and contact angle measurements, respectively. Fig. 1 shows the XPS spectra of the C 1s, N 1s, and S 2p regions for the Cys-b and OEG-thiol SAMs. The deconvoluted C 1s peak for the Cys-b SAM centered at 289.1 eV can be assigned to —O—C═O, indicating the presence of the carboxylate group in Cys-b [47,48]. The two distinct peaks at 286.5 and 285.0 eV in the C1s spectrum of the OEG-thiol SAM can be assigned as —O—C— and —C—C— in the OEG structure, respectively [49–51]. For the N 1s spectra, the Cys-b SAM shows a peak at 403.1 eV, which arises from the quaternary ammo-

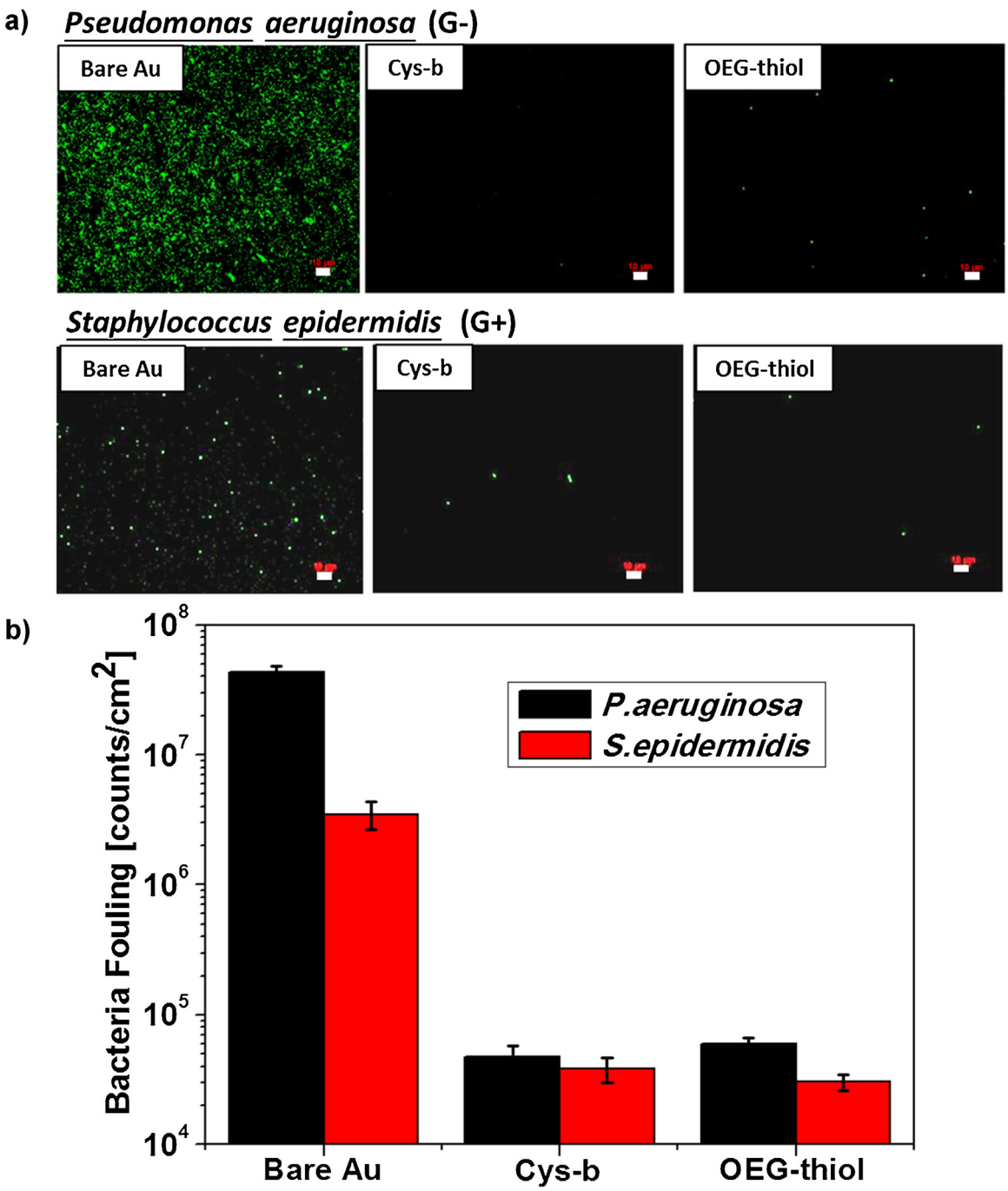

Fig. 3. Bacterial adsorption on samples of bare Au and Au modified with Cys-b and OEG-thiol. Gram-negative *P. aeruginosa* and gram-positive *S. epidermidis* were dissolved in PBS and incubated with substrates for 3 h at 37 °C. After washing with PBS, adsorbed bacteria were stained with Live/Dead dye and imaged with a fluorescence microscope (a). The quantitative results of bacteria numbers were estimated using ImageJ software (b). Scale bars in all images represent 10 μm.

nium in Cys-b. The observation of no peaks in the N 1s spectra of the OEG-thiol SAM is consistent with its chemical structure. The presence of bound sulfur for both types of SAMs was confirmed by the appearance of the S 2p peaks at 162.0 and 163.2 eV [46]. The ratio of S/N for Cys-b is close to 1, which was in agreement with the stoichiometry [37]. Herein, the peaks for oxidized sulfur and unbound thiols centered at 166.0 and 164.0 eV, respectively, were not observed in the two SAMs, indicating the efficient formation of SAMs on gold [46].

Fig. 2 shows the static contact angles for samples of bare gold and gold modified with Cys-b and OEG-thiol. The contact angles changed from $59 \pm 4^\circ$ for the unmodified substrate to $7 \pm 1^\circ$ and $21 \pm 3^\circ$ for the substrates modified with Cys-b and OEG-thiol, respectively, which is in agreement with previous studies [37,51]. Herein, due to strong ionic solvation, the Cys-b SAMs exhibited greater hydrophilicity than the OEG-thiol SAMs, consistent with a model in which the Cys-b-modified surfaces possess superhydrophilic characteristics with a tightly bound water layer. Notably, OEG, which interacts through hydrogen bonding with contacting water molecules, exhibits an amphiphilic nature that facilitates the dissolution of both aqueous and organic phases [52,53].

To test the capability of the coatings in fouling resistance, we exposed bare Au and Au modified with Cys-b and OEG-thiol to gram-negative *P. aeruginosa* and gram-positive *S. epidermidis* for

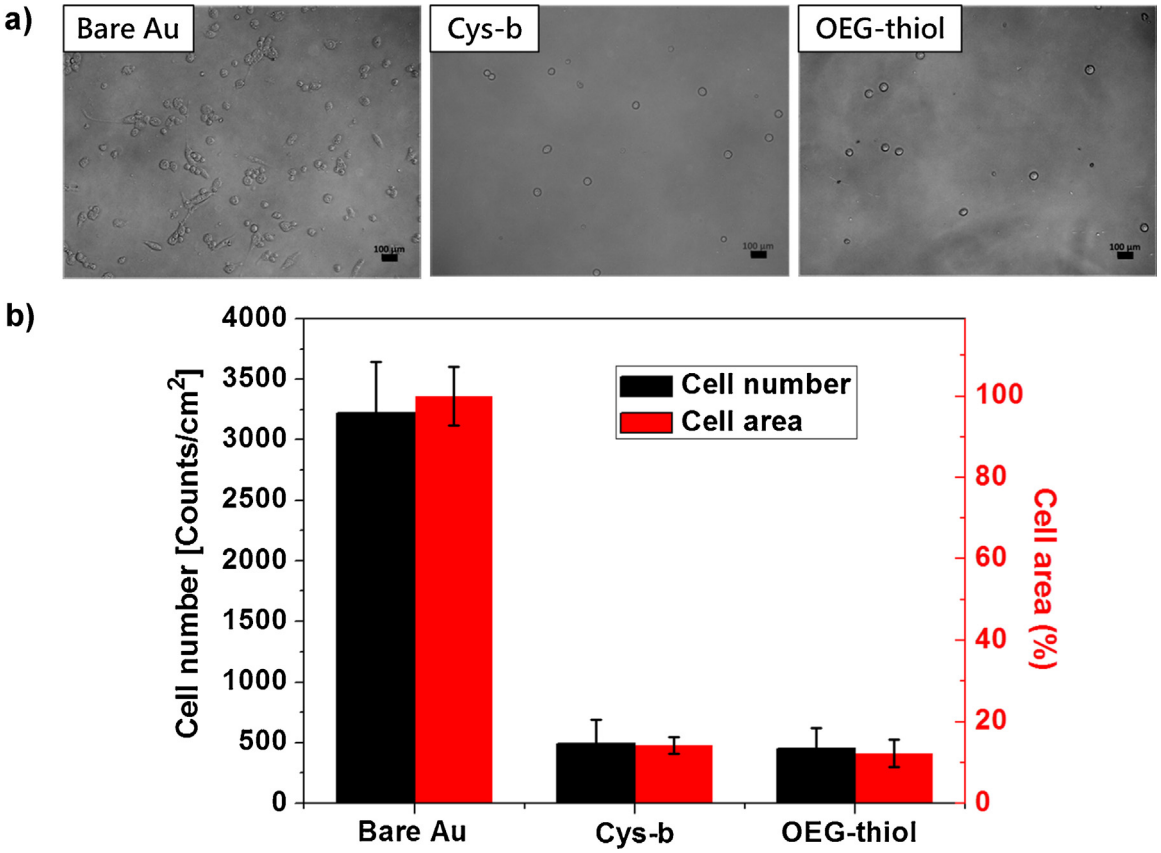

Fig. 4. The adhesion of 3T3 fibroblasts on bare Au and Au modified with Cys-b and OEG-thiol. The cells were cultured on samples in culture medium containing 1% FBS for 72 h at 37 °C. (a) After washing with PBS, images of the cells taken with optical microscopy. (b) Quantitative results of cell numbers and relative cell areas estimated using ImageJ software. The scale bars in all images represent 100 μm.

3 h at 37 °C. After gently washing with PBS to remove suspended and loosely bound bacteria, adhered bacteria were stained with Live/Dead dye for cell viability assays and imaged using fluorescence microscopy (Fig. 3a). Notably, the numbers of bacteria on the Cys-b and OEG-thiol SAMs were reduced with respect to the bare Au substrates for the two strains of bacteria. In addition, *P. aeruginosa* is more adhesive than *S. epidermidis*, manifested by a large amount of adhered *P. aeruginosa* on bare Au. The difference can be attributed to the higher expression level of the capsular exopolysaccharide of *P. aeruginosa*, which facilitates the adhesion of bacteria [54]. The quantitative results shown in Fig. 3b reveal that the numbers of the adsorbed *P. aeruginosa* and *S. epidermidis* were suppressed by about 3 and 2 orders of magnitude, respectively, compared with that on bare Au. In this work, the difference between Cys-b and OEG-thiol SAMs in antibacterial adhesion was insignificant.

The cell number and cell spreading area were determined to evaluate the cellular adaptation to the surface chemistries. In this study, NIH 3T3 fibroblasts were seeded on substrates of bare Au and Au modified with Cys-b and OEG-thiol, followed by culturing for 72 h. The cells were then washed with PBS to remove loosely bound cells and imaged using the bright-field microscopy (Fig. 4a), which showed that the numbers and cell spreading areas of fibroblasts on the substrates modified with Cys-b and OEG-thiol were lower than those on the bare Au substrate. In addition, the cells on the bare Au substrate exhibited bipolar shapes, whereas those on the Cys-b and OEG-thiol SAMs were round in appearance. The results indicated a reduction in cell adhesion and spreading dynamic equilibrium for the modified surfaces [55], reflecting the antifouling efficiency of the Cys-b and OEG-thiol coatings. The quantitative results are shown in Fig. 4b. The cell numbers were reduced by 85 and 86% on the SAMs derived from Cys-b and OEG-thiol, respectively, relative to the bare Au substrate. Moreover, the relative cell spreading areas on the SAMs derived from Cys-b and OEG-thiol were estimated to be 14 ± 2 and 12 ± 3%, respectively, relative to the bare Au substrate. In terms of the cell adhesion and growth, the two modified surfaces show no significant differences when compared to each other.

3.2. Modification of hollow gold-silver nanoshells

Hollow gold-silver nanoshells were coated with Cys-b and OEG-thiol, and the resultant materials were evaluated on the basis of optical properties, fouling resistance, colloidal stability, and function in hyperthermia applications. The extinction spectra of as-prepared nanoshells and nanoshells modified with Cys-b and OEG-thiol are shown in Fig. 5a. The extinction maximum of the modified nanoshells slightly red-shifted from 817 nm to 832 and 843 nm for the Cys-b-and OEG-modified nanoshells, respectively. The fouling resistance of the nanoshells was evaluated by DLS by measuring the increase in particle size as a function of the incubation time in the presence of the BSA solution. As shown in Fig. 5b, the fouling level of the as-prepared nanoshells is more prominent than that for modified nanoshells. After exposure to BSA for 5 h, the increment of the particle size for the as-prepared nanoshells is 315 ± 26 nm, whereas, those for the nanoshells modified with Cys-b and OEG-thiol were about 97 ± 26 and 99 ± 28 nm, which is roughly a 70% reduction compared with the unmodified sample. The increase in the particle sizes likely arises from the formation of protein corona and colloidal aggregation in the BSA solution. Note the concentration of BSA solution was adjusted to 4.9 mg/mL, which is about 10% that in human blood. The as-prepared nanoshells were

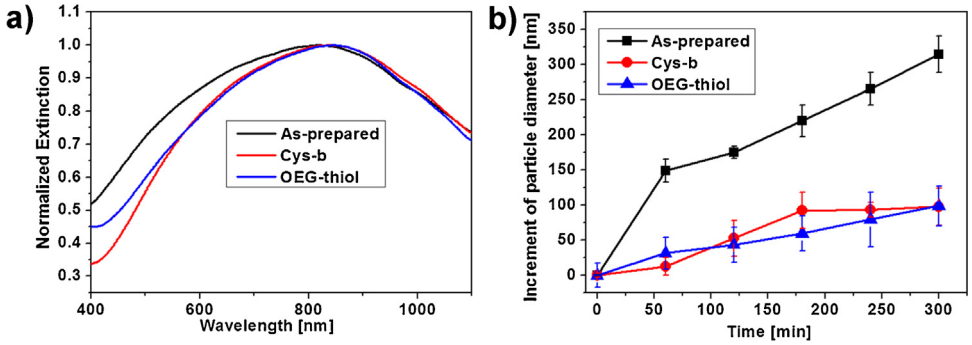

Fig. 5. (a) The extinction spectra of as-prepared, Cys-b-, and OEG-modified nanoshells. (b) DLS measurements of particle size as a function of incubation time in BSA solution.

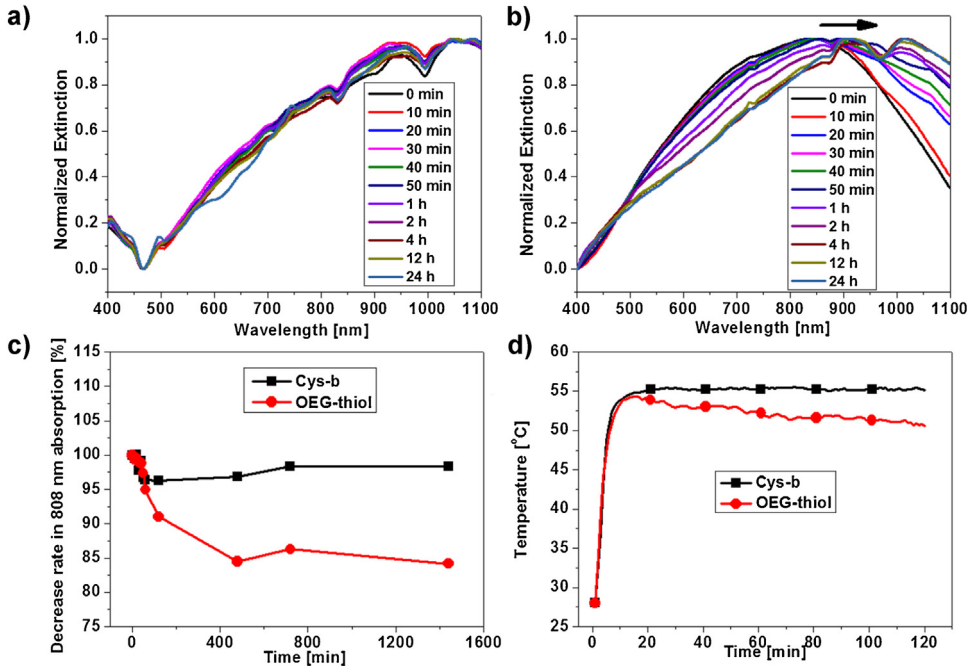

Fig. 6. Time evolution of the extinction spectra of nanoshells modified with (a) Cys-b and (b) OEG-thiol, where the samples were dissolved in 3 M NaCl solution, and the temperature was maintained at 50 °C. (c) Relative intensity of the extinction at 808 nm over 24 h. (d) Photolytic heating of nanoshell solutions by laser irradiation at 808 nm.

capped with citrate, which gives rise to a negatively charged surface that is colloidally stable in aqueous solution. Although the colloidal stability with citrate has been confirmed, the non-specific adsorption arising from electrostatic interactions cannot be excluded. In contrast, highly dispersed Cys-b-and OEG-modified nanoshells impart resistance to the adsorption of BSA, which can be attributed to the charge balance and hydrophilicity of the surface. Again, the differences between coatings derived from Cys-b and OEG-thiol appear to be insubstantial.

The plasmonic hollow gold-silver nanoshells were synthesized using established methods [40], by which the light extinction can be tuned from the visible to the NIR regions according to the size of particles and the composition of the alloy. The nanoshells with extinction in the NIR region at wavelengths of 800–1200 nm are particularly attractive for biomedical applications because the range of wavelengths is referred to as the "tissue transparency window" [56]. Thus, potential applications of nanoshells in nanomedicine, including photothermal cancer therapy [57–59] and photothermally triggered drug release, have been investigated [60,61]. However, for the full exploitation of nanodevices, the capping chemistry must be able to endure high temperature, strong light irradiation, and complex biological environments.

OEG-based SAMs have been employed as a model surface for studying biorecognition processes by taking advantage of well-defined compositions and control over molecular adsorption. Thus, OEG-thiol SAMs play important roles in a variety of biosensing applications when coupled with analytical techniques such as SPR spectroscopy [62,63], optical ellipsometry [64], and quartz crystal microbalance [65]. In addition, the capability to spatially decorate the surfaces into a microscale array facilitates high-throughput screening for new drugs, biomarkers, and diagnostic techniques [66,67]. Importantly, when compared to OEG-thiol, our new superhydrophilic zwitterionic ligand, Cys-b, shows comparable antifouling properties against the adsorption of proteins, bacteria, NIH 3T3 fibroblasts. In addition, the molecular weight of Cys-b (163 Da) is smaller than OEG-thiol (336 Da), leading to smaller hydrodynamic sizes of nanoparticles coated with Cys-b-coated. In addition, Cys-b resists the photoinduced oxidation to the amino group of Cys and also provides better tolerance toward pH changes to maintain its zwitterionic character [37]. The colloidal stability and optical properties of the Cys-b-modified nanoparticles show no significant differences with OEG-modified samples under our experimental conditions. Consequently, Cys-b can serve as an alternative to OEG-thiol analogs, and its unique features of

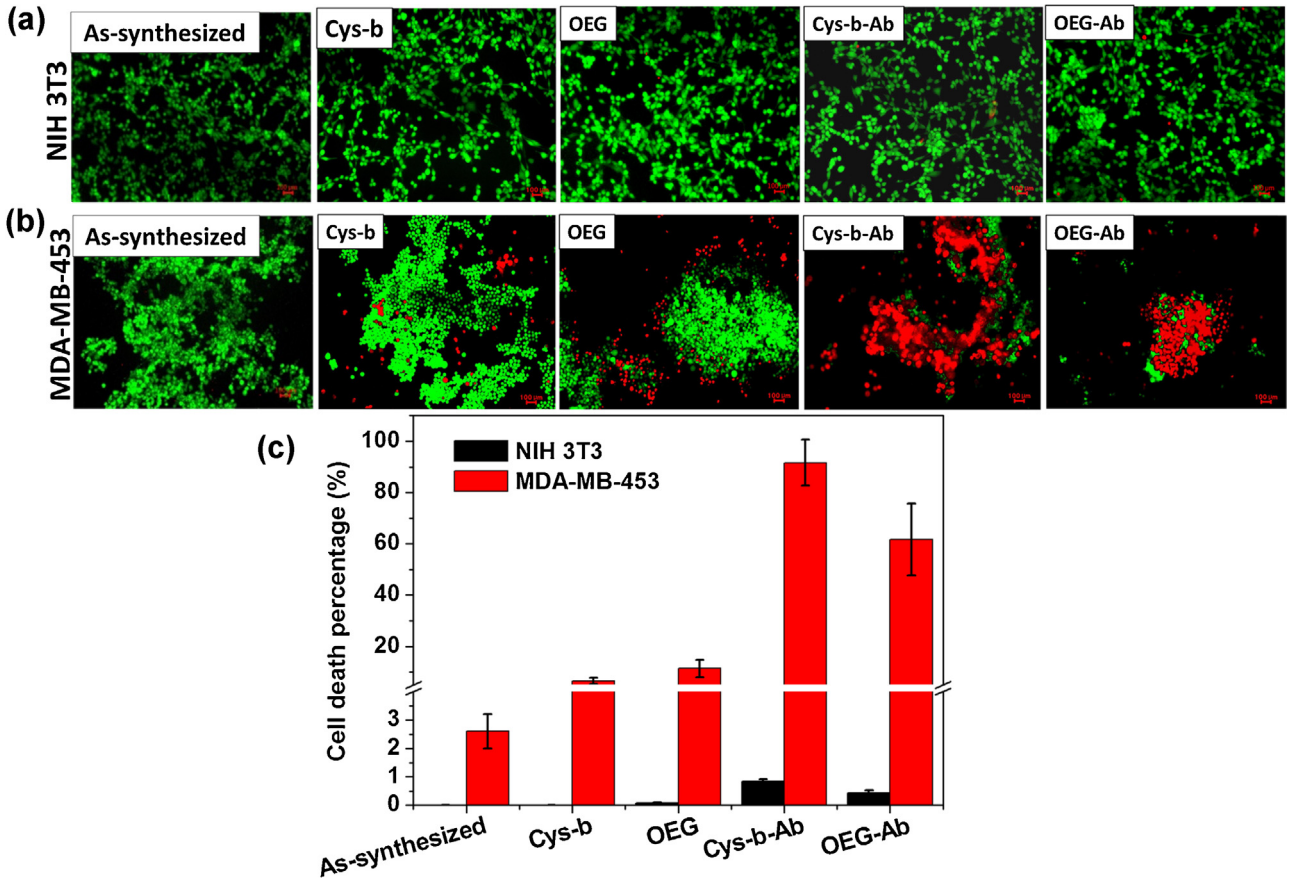

Fig. 7. Nanoshell-assisted NIR plasmonic hyperthermia for HER2-negative NIH 3T3 and HER2-positive MDA-MB-453 cells. (a) Fluorescence images of NIH 3T3 fibroblasts treated with as-synthesized nanoshells and nanoshells modified with Cys-b and OEG-thiol and those conjugated with anti-HER2 antibodies, after irradiation of NIR light. (b) Fluorescence images of MDA-MB-453 cells with the same treatments as NIH 3T3. Viable cells were stained green with calcein, and dead cells were stained red with EthD-1. Scale bars represent 100 μm. (c) Quantitative cell death percentages for NIH 3T3 and MDA-MB-453 cells with different modified nanoshells (for interpretation of the references to colour in this figure legend, the reader is referred to the web version of this article).

superhydrophilicity, photostability, ultra-small size, and environmental insusceptibility make it a particularly attractive nanoscale coating material.

To verify the colloidal stability of modified nanoshells in the presence of the high ionic strength and heat, the nanoshells modified with Cys-b and OEG-thiol were dissolved in 3 M NaCl solution, and the temperature was maintained at 50 °C, which is comparable to the temperature of solutions containing nanoshells exposed to NIR irradiation at a power density of 4.6 W/cm^2 for 10 min. The extinction spectra were then recorded over 24 h at 50 °C. Fig. 6a,b shows that the SPR peaks of the nanoshells modified with Cys-b were optically constant with time; in contrast, the nanoshells coated with OEG-thiol underwent a red shift with time. Furthermore, Fig. 6c shows a systematically decreasing ratio of the extinction intensities at 808 nm as a function of irradiation time for the two samples. After 12 h of heating in 3 M NaCl solution, the extinction intensity of the OEG-modified nanoshells decreased by 16%. In a related study, NIR light at 808 nm was used for photolytic heating of the nanoshells in solution over the course of 2 h (see Fig. 6d). This experiment showed that the temperature of the solution can be increased to ~54 °C within 15 min for nanoshell samples modified with both Cys-b and OEG-thiol. After reaching the peak temperature, the temperature plateaued for the Cys-b sample, which likely reflects temperature equilibrium between heat generation from nanoshells and heat loss to the environment. In contrast, the temperature of the OEG-thiol sample gradually decreased with the irradiation time, which likely arises from a loss of photothermal performance due to particle aggregation and precipitation. The latter hypothesis can perhaps be supported by the fact that OEG exhibits a lower critical solution temperature (LCST), leading to dehydration and consequent failure to prevent aggregation at high temperature in salt solutions [27].

3.3. Hyperthermia treatments for cancer cells

HER2, which is highly expressed in a significant proportion of breast cancer, ovarian cancer, and gastric cancer, is a ligand for delivery of therapeutic carriers [68–70]. Therefore, the HER2 mAb-conjugated hollow Au-Ag nanoshells were synthesized to target the HER2-positive MDA-MB-453 breast cancer cells for hyperthermia treatment under NIR irradiation. Surface functionalization was conducted by mixing bio-inert capping ligand (i.e., Cys-b or OEG-thiol) with a functionalizable carboxylate-terminated ligand (i.e., COOH-thiol). The carboxylic acid can be activated by the EDC/NHS amine coupling chemistry [71,72]. It was postulated that the carboxylate group in Cys-b could also serve as a functional group for protein conjugation as CB-associated polymers [52,73,74]. However, because of the limited accessibility and low pKa of the carboxylate group in Cys-b, the efficiency of bioconjugation is largely impracticable. Therefore, we utilized the COOH-thiol as a functional ligand for effective conjugation with antibodies. Nanoshells modified with Cys-b and OEG-thiol both with and without mAb conjugation were incubated with MDA-MB-453 and NIH 3T3 at 37 °C for 2 h, followed by washing with PBS and NIR irradiation for

10 min. The as-synthesized nanoshells without further modification were used as a control sample. Fig. 7 provides the photographs and numerical data for live and dead cells analyzed using fluorescence microscopy. Figs. 7a and bshow that the NIH 3T3 fibroblasts were largely unaffected by NIR irradiation, which is likely due to the limited uptake of nanoshells with modification of the Cys-b and OEG-thiol coatings. Notably, the uptake can be plausibly inhibited by the antifouling properties of the Cys-b and OEG-thiol coatings. In contrast, MDA-MB-453 cells were treated with anti-HER2 mAb-conjugated nanoshells. Fig. 7b shows that the MDA-MB-453 cells were damaged after exposure to NIR, while the fibroblasts remained largely intact. The quantitative cell death percentages are shown in Fig. 7c. After NIR radiation, 92 ± 9 and $62 \pm 14\%$ of the MDA-MB-453 cells were killed upon treatment with Ab-conjugated nanoshells modified with Cys-b and OEG-thiol, respectively. In contrast, less than one percent of the NIH 3T3 cells were killed under the same conditions. Thus, the results confirmed the selective delivery of anti-HER2 mAb-conjugated nanoshells into cancer cells through ligand-receptor mediated endocytosis. In addition, nanoshells modified with Cys-b exhibited better thermal ablation of the MDA-MB-453 cells than nanoshells modified with OEG-thiol, likely due to the enhanced photothermal stability and effective delivery of the Cys-b nanoshells. Moreover, small portions (~10%) of MDA-MB-453 cells were dead after treatment with nanoshells modified with Cys-b and OEG-thiol having no Ab conjugation after sequential NIR irradiation, which we attribute to poor uptake of the nanoshells and/or weak tolerance of the cells to the NIR-induced heat. Consequently, these studies demonstrate the promising use of the Ab-conjugated hollow gold-silver nanoshells modified with Cys-b as an effective and specific tumor ablation agent.

4. Conclusions

This manuscript describes the evaluation of a new bio-derived antifouling adsorbate, Cys-b, for the modification of plasmonic hollow Au-Ag nanoshells for the hyperthermia treatment of HER2-positive MDA-MB-453 breast cancer cells. Superhydrophilic coatings of Cys-b on Au substrates displayed comparable antifouling properties with conventional OEG-based SAMs, manifested as considerable reduction in bacterial adsorption and adhesion of NIH 3T3 fibroblasts. In addition, nanoshells modified with Cys-b exhibited better colloidal stability and photothermal properties at high ionic strength and temperature than those modified with OEG-thiol, indicating that the unique hydration properties of zwitterionic Cys-b are insusceptible to environmental stimuli. In addition, anti-HER2 antibodies were chemically functionalized onto nanoshells modified with Cys-b for the development of an effective and specific tumor ablation agent for the hyperthermia treatment of MDA-MB-453 breast cancer cells. The results indicated that over 90% of the cells were killed after NIR irradiation for 10 min. Consequently, zwitterionic Cys-b as a nanoscale coating material offers great potential in a wide range of bio-applications.

Acknowledgments

The authors acknowledge the Ministry of Science and Technology (MOST 104-2221-E-008-108) for financial support of this project. Research efforts at the University of Houston were generously supported by the National Science Foundation (CHE-1411265), the Robert A. Welch Foundation (E-1320), and the Texas Center for Superconductivity at the University of Houston. We thank Ishwar Kumar Mishra for assistance with the nanoshell concentration measurements (NanoSight NS300).

Appendix A. Supplementary data

Supplementary data associated with this article can be found, in the online version, at http://dx.doi.org/10.1016/j.colsurfb.2016.05.004.

References

[1] X.H. Huang, P.K. Jain, I.H. El-Sayed, M.A. El-Sayed, Plasmonic photothermal therapy (PPTT) using gold nanoparticles, Lasers Med. Sci. 23 (2008) 217–228.
[2] T. Refaat, S. Sachdev, V. Sathiaseelan, I. Helenowski, S. Abdelmoneim, M.C. Pierce, G. Woloschak, W. Small, B. Mittal, K.D. Kiel, Hyperthermia and radiation therapy for locally advanced or recurrent breast cancer, Breast 24 (2015) 418–425.
[3] X.M. Liu, H. Chen, X.D. Chen, Y. Alfadhl, J.S. Yu, D.S. Wen, Radiofrequency heating of nanomaterials for cancer treatment: progress, controversies, and future development, Appl. Phys. Rev. 2 (2015) 011103.
[4] D.L. Shi, M.E. Sadat, A.W. Dunn, D.B. Mast, Photo-fluorescent and magnetic properties of iron oxide nanoparticles for biomedical applications, Nanoscale 7 (2015) 8209–8232.
[5] J. Majeed, L. Pradhan, R.S. Ningthoujam, R.K. Vatsa, D. Bahadur, A.K. Tyagi, Enhanced specific absorption rate in silanol functionalized Fe_3O_4 core-shell nanoparticles: study of Fe leaching in Fe3O4 and hyperthermia in L929 and HeLa cells, Colloid Surf. B-Biointerfaces 122 (2014) 396–403.
[6] T.T. Sun, J. Qi, M. Zheng, Z.G. Xie, Z.Y. Wang, X.B. Jing, Thiadiazole molecules and poly(ethylene glycol)-block-polylactide self-assembled nanoparticles as effective photothermal agents, Colloid Surf. B-Biointerfaces 136 (2015) 201–206.
[7] M.A. Yaseen, J. Yu, M.S. Wong, B. Anvari, Stability assessment of indocyanine green within dextran-coated mesocapsules by absorbance spectroscopy, J. Biomed. Opt 12 (2007) 64031.
[8] P.R. Jheng, K.Y. Lu, S.H. Yu, F.L. Mi, Free DOX and chitosan-*N*-arginine conjugate stabilized indocyanine green nanoparticles for combined chemophotothermal therapy, Colloid Surf. B-Biointerfaces 136 (2015) 402–412.
[9] E. Boisselier, D. Astruc, Gold nanoparticles in nanomedicine: preparations, imaging, diagnostics, therapies and toxicity, Chem. Soc. Rev. 38 (2009) 1759–1782.
[10] J.H. Gao, H.W. Gu, B. Xu, Multifunctional magnetic aanoparticles: design, synthesis, and biomedical applications, Accounts Chem. Res. 42 (2009) 1097–1107.
[11] D. Ling, N. Lee, T. Hyeon, Chemical synthesis and assembly of uniformly sized iron oxide nanoparticles for medical applications, Accounts Chem. Res. 48 (2015) 1276–1285.
[12] I.H. El-Sayed, X.H. Huang, M.A. El-Sayed, Selective laser photo-thermal therapy of epithelial carcinoma using anti-EGFR antibody conjugated gold nanoparticles, Cancer Lett. 239 (2006) 129–135.
[13] K. Fang, L.N. Song, Z.X. Gu, F. Yang, Y. Zhang, N. Gu, Magnetic field activated drug release system based on magnetic PLGA microspheres for chemo-thermal therapy, Colloid Surf. B-Biointerfaces 136 (2015) 712–720.
[14] E.R. Riva, A. Desii, E. Sinibaldi, G. Ciofani, V. Piazza, B. Mazzolai, V. Mattoli, Gold nanoshell/polysaccharide nanofilm for controlled laser-assisted tissue thermal ablation, ACS Nano 8 (2014) 5552–5563.
[15] C.H. Li, A.C. Jamison, S. Rittikulsittichai, T.C. Lee, T.R. Lee, In situ growth of hollow gold-silver nanoshells within porous silica offers tunable plasmonic extinctions and enhanced colloidal stability, ACS Appl. Mater. Interfaces 6 (2014) 19943–19950.
[16] J.F. Liao, W.T. Li, J.R. Peng, Q. Yang, H. Li, Y.Q. Wei, X.N. Zhang, Z.Y. Qian, Combined cancer photothermal-chemotherapy based on doxorubicin/gold nanorod-loaded polymersomes, Theranostics 5 (2015) 345–356.
[17] T.B. Huff, L. Tong, Y. Zhao, M.N. Hansen, J.X. Cheng, A. Wei, Hyperthermic effects of gold nanorods on tumor cells, Nanomedicine 2 (2007) 125–132.
[18] J.Y. Chen, B. Wiley, Z.Y. Li, D. Campbell, F. Saeki, H. Cang, L. Au, J. Lee, X.D. Li, Y.N. Xia, Gold nanocages: engineering their structure for biomedical applications, Adv. Mater. 17 (2005) 2255–2261.
[19] X.M. Yi, F.L. Wang, W.J. Qin, X.J. Yang, J.L. Yuan, Near-infrared fluorescent probes in cancer imaging and therapy: an emerging field, Int. J. Nanomed. 9 (2014) 1347–1365.
[20] J.V. Jokerst, T. Lobovkina, R.N. Zare, S.S. Gambhir, Nanoparticle PEGylation for imaging and therapy, Nanomedicine 6 (2011) 715–728.
[21] K. Knop, R. Hoogenboom, D. Fischer, U.S. Schubert, Poly(ethylene glycol) in drug delivery: pros and cons as well as potential alternatives, Angew. Chem.-Int. Edit. 49 (2010) 6288–6308.
[22] S.I. Jeon, J.H. Lee, J.D. Andrade, P.G. Degennes, Protein surface interactions in the presence of polyethylene oxide. 1. Simplified theory, J. Colloid Interface Sci. 142 (1991) 149–158.
[23] S.I. Jeon, J.D. Andrade, Protein surface interactions in the presence of polyethylene oxide. 2. Effect of protein size, J. Colloid Interface Sci. 142 (1991) 159–166.
[24] P. Harder, M. Grunze, R. Dahint, G.M. Whitesides, P.E. Laibinis, Molecular conformation in oligo(ethylene glycol)-terminated self-assembled monolayers on gold and silver surfaces determines their ability to resist protein adsorption, J. Phys. Chem. B 102 (1998) 426–436.

[25] Q.G. Xu, L.M. Ensign, N.J. Boylan, A. Schön, X.Q. Gong, J.C. Yang, N.W. Lamb, S.T. Cai, T. Yu, E. Freirem, J. Hanes, Impact of surface polyethylene glycol (PEG) density on biodegradable nanoparticle transport in mucus ex vivo and distribution in vivo, ACS Nano 9 (2015) 9217–9227.
[26] M. Ataman, Properties of aqueous salt solutions of poly(ethylene oxide). Cloud points, θ temperatures, Colloid. Polym. Sci. 265 (1987) 19–25.
[27] Z.G. Estephan, P.S. Schlenoff, J.B. Schlenoff, Zwitteration as an alternative to PEGylation, Langmuir 27 (2011) 6794–6800.
[28] R.S. Porter, A. Casale, Recent studies of polymer reactions caused by stress, Polym. Eng. Sci. 25 (1985) 129–156.
[29] S. Morlat, J.L. Gardette, Phototransformation of water-soluble polymers. I: photo- and thermooxidation of poly(ethylene oxide) in solid state, Polymer 42 (2001) 6071–6079.
[30] Q. Shao, S.Y. Jiang, Molecular understanding and design of zwitterionic materials, Adv. Mater. 27 (2015) 15–26.
[31] S.Y. Jiang, Z.Q. Cao, Ultralow-fouling, functionalizable, and hydrolyzable zwitterionic materials and Their derivatives for biological applications, Adv. Mater. 22 (2010) 920–932.
[32] R.E. Holmlin, X.X. Chen, R.G. Chapman, S. Takayama, G.M. Whitesides, Zwitterionic SAMs that resist nonspecific adsorption of protein from aqueous buffer, Langmuir 17 (2001) 2841–2850.
[33] M.C. Sin, P.T. Lou, C.H. Cho, A. Chinnathambi, S.A. Alharbi, Y. Chang, An intuitive thermal-induced surface zwitterionization for versatile, well-controlled haemocompatible organic and inorganic materials, Colloid Surf. B-Biointerfaces 127 (2015) 54–64.
[34] S.F. Chen, S.Y. Jiang, A new avenue to nonfouling materials, Adv. Mater. 20 (2008) 335–338.
[35] M.T. Cai, M.T. Leng, A.J. Lu, L. He, X.X. Xie, L. Huang, Y.H. Ma, J. Cao, Y.W. Chen, X.L. Luo, Synthesis of amphiphilic copolymers containing zwitterionic sulfobetaine as pH and redox responsive drug carriers, Colloid Surf. B-Biointerfaces 126 (2015) 1–9.
[36] C.J. Huang, L.C. Wang, Bio-inspired multifunctional catecholic assembly for photo-programmable biointerface, Colloid Surf. B-Biointerfaces 134 (2015) 247–253.
[37] C.J. Huang, S.H. Chu, L.C. Wang, C.H. Li, T.R. Lee, Bio-inspired zwitterionic surface assembly with robust photostability and fouling resistance, ACS Appl. Mater. Interfaces 7 (2015) 23776–23786.
[38] H. Wang, S. Chen, L. Li, S. Jiang, Improved method for the preparation of carboxylic acid and amine terminated self-assembled monolayers of alkanethiolates, Langmuir 21 (2005) 2633–2636.
[39] P.C. Lee, D. Meisel, Adsorption and surface-enhanced raman of dyes on silver and gold sols, J. Phys. Chem. 86 (1982) 3391–3395.
[40] V. Vongsayat, B.M. Vittur, W.W. Bryan, J.H. Kim, T.R. Lee, Ultrasmall hollow gold-Silver nanoshells with extinctions strongly red-shifted to the near-Infrared, ACS Appl. Mater. Interfaces 3 (2011) 3616–3624.
[41] S.J. Oldenburg, R.D. Averitt, S.L. Westcott, N.J. Halas, Nanoengineering of optical resonances, Chem. Phys. Lett. 288 (1998) 243–247.
[42] H. Tumturk, F. Sahin, E. Turan, Magnetic nanoparticles coated with different shells for biorecognition: high specific binding capacity, Analyst 139 (2014) 1093–1100.
[43] L.X. Tiefenauer, G. Kuhne, R.Y. Andres, Antibody magnetite nanoparticles-in-vitro characterization of a potential tumor-specific contrast agent for magnetic resonance imaging, Bioconjugate Chem. 4 (1993) 347–352.
[44] N. Dinauer, S. Balthasar, C. Weber, J. Kreuter, K. Langer, H. von Briesen, Selective targeting of antibody-conjugated nanoparticles to leukemic cells and primary T-lymphocytes, Biomaterials 26 (2005) 5898–5906.
[45] K. Uvdal, P. Bodo, B. Liedberg, L-Cysteine adsorbed on gold and copper—an X-ray photoelectron-spectroscopy study, J. Colloid Interface Sci. 149 (1992) 162–173.
[46] H. Wang, S.F. Chen, L.Y. Li, S.Y. Jiang, Improved method for the preparation of carboxylic acid and amine terminated self-assembled monolayers of alkanethiolates, Langmuir 21 (2005) 2633–2636.
[47] Z. Zhang, T. Chao, S.F. Chen, S.Y. Jiang, Superlow fouling sulfobetaine and carboxybetaine polymers on glass slides, Langmuir 22 (2006) 10072–10077.
[48] C.L. He, Y.L. Liu, Z.P. Xue, M.T. Zheng, H.B. Wang, Y. Xiao, H.W. Dong, H.R. Zhang, B.F. Lei, Simple synthesis of carboxylate-rich porous carbon microspheres for high-performance supercapacitor electrode materials, Int. J. Electrochem. Sci. 8 (2013) 7088–7098.
[49] S. Sharma, R.W. Johnson, T.A. Desai, XPS and AFM analysis of antifouling PEG interfaces for microfabricated silicon biosensors, Biosens. Bioelectron. 20 (2004) 227–239.
[50] K.C. Popat, S. Sharma, T.A. Desai, Quantitative XPS analysis of PEG-modified silicon surfaces, J. Phys. Chem. B 108 (2004) 5185–5188.
[51] M. Cerruti, S. Fissolo, C. Carraro, C. Ricciardi, A. Majumdar, R. Maboudian, Poly(ethylene glycol) monolayer formation and stability on gold and silicon nitride substrates, Langmuir 24 (2008) 10646–10653.
[52] Z.Q. Cao, S.Y. Jiang, Super-hydrophilic zwitterionic poly(carboxybetaine) and amphiphilic non-ionic poly(ethylene glycol) for stealth nanoparticles, Nano Today 7 (2012) 404–413.
[53] Z.Q. Cao, L. Zhang, S.Y. Jiang, Superhydrophilic zwitterionic polymers stabilize liposomes, Langmuir 28 (2012) 11625–11632.
[54] C.J. Huang, L. Mi, S.Y. Jiang, Interactions of alginate-producing and -deficient *Pseudomonas aeruginosa* with zwitterionic polymers, Biomaterials 33 (2012) 3626–3631.
[55] E. Cukierman, R. Pankov, K.M. Yamada, Cell interactions with three-dimensional matrices, Curr. Opin. Cell Biol. 14 (2002) 633–639.
[56] C.R. Simpson, M. Kohl, M. Essenpreis, M. Cope, Near-infrared optical properties of ex vivo human skin and subcutaneous tissues measured using the Monte Carlo inversion technique, Phys. Med. Biol. 43 (1998) 2465–2478.
[57] X.Y. Zhang, Gold nanoparticles: recent advances in the biomedical applications, Cell Biochem. Biophys. 72 (2015) 771–775.
[58] Y.P. Gao, Y.S. Li, J.Z. Chen, S.J. Zhu, X.H. Liu, L.P. Zhou, P. Shi, D.C. Niu, J.L. Gu, J.L. Shi, Multifunctional gold nanostar-based nanocomposite: synthesis and application for noninvasive MR-SERS imaging-guided photothermal ablation, Biomaterials 60 (2015) 31–41.
[59] X.H. Huang, I.H. El-Sayed, W. Qian, M.A. El-Sayed, Cancer cell imaging and photothermal therapy in the near-infrared region by using gold nanorods, J. Am. Chem. Soc. 128 (2006) 2115–2120.
[60] J.J. Shi, L. Wang, J. Zhang, R. Ma, J. Gao, Y. Liu, C.F. Zhang, Z.Z. Zhang, A tumor-targeting near-infrared laser-triggered drug delivery system based on GO@Ag nanoparticles for chemo-photothermal therapy and X-ray imaging, Biomaterials 35 (2014) 5847–5861.
[61] M. Das, N. Sanson, D. Fava, E. Kumacheva, Microgels loaded with gold nanorods: photothermally triggered volume transitions under physiological conditions, Langmuir 23 (2007) 196–201.
[62] C.J. Huang, J. Dostalek, W. Knoll, Optimization of layer structure supporting long range surface plasmons for surface plasmon-enhanced fluorescence spectroscopy biosensors, J. Vac. Sci. Technol. B 28 (2010) 66–72.
[63] C.J. Huang, J. Dostalek, A. Sessitsch, W. Knoll, Long-range surface plasmon-enhanced fluorescence spectroscopy biosensor for ultrasensitive detection of *E. coli* O157:H7, Anal. Chem. 83 (2011) 674–677.
[64] C. Hoffmann, G.E.M. Tovar, Mixed self-assembled monolayers (SAMs) consisting of methoxy-tri(ethylene glycol)-terminated and alkyl-terminated dimethylchlorosilanes control the non-specific adsorption of proteins at oxidic surfaces, J. Colloid Interface Sci. 295 (2006) 427–435.
[65] E. Nileback, L. Feuz, H. Uddenberg, R. Valiokas, S. Svedhem, Characterization and application of a surface modification designed for QCM-D studies of biotinylated biomolecules, Biosens. Bioelectron. 28 (2011) 407–413.
[66] P.K. Ajikumar, J. Kiat, Y.C. Tang, J.Y. Lee, G. Stephanopoulos, H.P. Too, Carboxyl-terminated dendrimer-coated bioactive interface for protein microarray: high-sensitivity detection of antigen in complex biological samples, Langmuir 23 (2007) 5670–5677.
[67] Z.Z. Wang, T. Wilkop, J.H. Han, Y. Dong, M.J. Linman, Q. Cheng, Development of air-stable, supported membrane arrays with photolithography for study of phosphoinositide-protein interactions using surface plasmon resonance imaging, Anal. Chem. 80 (2008) 6397–6404.
[68] R. Vivek, R. Thangam, S.R. Kumar, C. Rejeeth, S. Sivasubramanian, S. Vincent, D. Gopi, S. Kannan, HER2 targeted breast cancer therapy with switchable off/on multifunctional smart magnetic polymer core-shell nanocomposites, ACS Appl. Mater. Interfaces 8 (2016) 2262–2279.
[69] R. Huang, Y. Sun, Q.H. Gao, Q.C. Wang, B.W. Sun, Trastuzumab-mediated selective delivery for platinum drug to HER2-positive breast cancer cells, Anticancer Drugs 26 (2015) 957–963.
[70] H.W. Chen, L.Y. Wang, Q.Q. Yu, W.P. Qian, D. Tiwari, H. Yi, A.Y. Wang, J. Huang, L.L. Yang, H. Mao, Anti-HER2 antibody and ScFvEGFR-conjugated antifouling magnetic iron oxide nanoparticles for targeting and magnetic resonance imaging of breast cancer, Int. J. Nanomed. 8 (2013) 3781–3794.
[71] K. Kerman, D. Ozkan, P. Kara, B. Meric, J.J. Gooding, M. Ozsoz, Voltammetric determination of DNA hybridization using methylene blue and self-assembled alkanethiol monolayer on gold electrodes, Anal. Chim. Acta 462 (2002) 39–47.
[72] M.J.B. Wissink, R. Beernink, J.S. Pieper, A.A. Poot, G.H.M. Engbers, T. Beugeling, W.G. van Aken, J. Feijen, Immobilization of heparin to EDC/NHS-crosslinked collagen. Characterization and in vitro evaluation, Biomaterials 22 (2001) 151–163.
[73] C.J. Huang, N.D. Brault, Y.T. Li, Q.M. Yu, S.Y. Jiang, Controlled hierarchical architecture in surface-initiated zwitterionic polymer brushes with structurally regulated functionalities, Adv. Mater. 24 (2012) 1834–1837.
[74] C.J. Huang, Y.T. Li, S.Y. Jiang, Zwitterionic polymer-based platform with two-layer architecture for ultra low fouling and high protein loading, Anal. Chem. 84 (2012) 3440–3445.